MOX-Report No. 22/2021

Fluid structure interaction analysis to stratify the behavior of different atheromatous carotid plaques

Domanin, M.; Bennati, L.; Vergara, C.; Bissacco, D.; Malloggi, C.; Silani, V.; Parati, G.; Trimarchi, S.; Casana, R.

MOX, Dipartimento di Matematica
Politecnico di Milano, Via Bonardi 9 - 20133 Milano (Italy)

mox-dmat@polimi.it http://mox.polimi.it

FLUID STRUCTURE INTERACTION ANALYSIS TO STRATIFY THE BEHAVIOR OF DIFFERENT ATHEROMATOUS CAROTID PLAQUES

Maurizio Domanin [1,2], Lorenzo Bennati [3], Christian Vergara [4], Daniele Bissacco [1], Chiara Malloggi [5], Vincenzo Silani [5,6], Gianfranco Parati [7,8], Santi Trimarchi [1,2], Renato Casana [9,10]

Affiliations

1 Dipartimento di Scienze Cliniche e di Comunità, Università degli Studi di Milano, Milan, Italy.
2 Vascular Surgery Unit, IRCCS Ospedale Maggiore Policlinico, Milan, Italy.
3 Dipartimento di Scienze Chirurgiche Odontostomatologiche e Materno-Infantili, Università degli Studi di Verona, Italy
4 LABS, Dipartimento di Chimica, Materiali e Ingegneria Chimica "Giulio Natta", Politecnico di Milano, Milan, Italy.
5 Istituto Auxologico Italiano, IRCCS, Dipartimento di Neurologia e Stroke Unit e Laboratorio di Ricerche di Neuroscienze, Ospedale San Luca, Milano, Italy.
6 Dipartimento di Fisiopatologia Medico-Chirurgica e dei Trapianti, Centro 'Dino Ferrari', Università degli Studi di Milano, Milano, Italy.
7 Istituto Auxologico Italiano, IRCCS, Dipartimento di Scienze Cardiovascolari, Neurologiche, Metaboliche, Ospedale San Luca, Milano, Italy.
8 Dipartimento di Medicina e Chirurgia, Università di Milano-Bicocca, Milano, Italy.
9 Istituto Auxologico Italiano, IRCCS, Centro Chirurgia Vascolare, Auxologico Capitanio, Milano, Italy.
10 Istituto Auxologico Italiano, IRCCS, Laboratorio Sperimentale di Ricerche di Chirurgia Vascolare, Milano, Italy.

Corresponding Author:

Maurizio Domanin,
maurizio.domanin@unimi.it

Dipartimento di Scienze Cliniche e di COmunità (DISCCO) – Università di Milano - ITALY
Vascular Surgery Unit, Fondazione Ca' Granda Ospedale Maggiore Policlinico, Via Sforza 35, 20122 Milano, Italy. Tel. +39-2-55032438

Key words: Carotid Stenosis; Carotid Plaque; Carotid Endarterectomy; Computational Fluid Dynamics; Fluid Structure Interaction; Risk Stratification.

ABSTRACT (294 words)

Objectives: Different plaque types could have different hemodynamic and structural behaviors in asymptomatic carotid stenosis (ACS), increasing the risk of instability.

Methods: The vessel lumen, the wall, and the geometries of three different types of carotid plaques, namely lipid (LP), fibrous (FP), and calcific (CP) were reconstructed starting with CTA images from 15 candidate patients for carotid revascularization with ACS >70%, in order to obtain 5 models for each type. Fluid structure interaction (FSI) analyses were performed to describe hemodynamic and structural behavior in different types of plaques by computing wall shear stresses (WSS), plaque displacements (D), von Mises stresses (VMS), and absorbed elastic energy (AEE) spatial distribution and their maximum-in-space values at the systolic peak, namely WSS_{syst}, D_{syst}, VMS_{syst} and AEE_{syst}.

Results: WSS_{syst} resulted significantly lower in LP, whereas in FP we found intermediate values (+33%) and the highest WSS_{syst} (+157%) in CP. The highest values of D_{syst} were observed in LP, with a different spatial distribution, being localized mainly in the inner region of the thin fibrous cap, at the shoulder of the stenosis, whereas for FP and CP the values were -250% and -480% lower, respectively. VMS_{syst} in the LP group was again localized to the inner region of the thin fibrous cap, whereas FP and CP had lower values, -150% and -400%, respectively, without spatial concentration of peak stresses. AEE_{syst} was determined to be focused at the fibrous cap, and capable of storing elevated values of energy due to the compliant nature of the inner core in LP, while lower values were found for FP and CP, -470% and -2240%, respectively.

Conclusions: Depending upon their nature, plaques store different amounts of mechanical energy. The deformation causes different distributions of internal forces inside the plaque, thus influencing vulnerability properties, especially for LP.

Key words 3-6 CAROTID STENOSIS, CAROTID PLAQUE, CAROTID ENDARTERECTOMY, COMPUTATIONAL FLUID DYNAMICS, FLUID STRUCTURE INTERACTION, RISK STRATIFICATION

Word count: 3938

What this paper adds:

The measurement of mechanical descriptors such as von Mises stress and, for the first time to the best of our knowledge, the absorbed energy can give better insights on different vulnerability conditions of carotid plaques, thus contributing to a better understanding of the behavior of asymptomatic carotid plaques in relation to their physical nature.

INTRODUCTION

Cerebral ischemic stroke is one of the leading causes of debilitating neurological disease and death. Large-vessel cervical or intracranial atherosclerosis is the cause of 16% of all ischemic strokes attributed to carotid artery stenosis.[1]

The surgical treatment of asymptomatic carotid stenosis (ACS) remains controversial. Currently, the major guidelines still advise carotid revascularization in asymptomatic patients when >60% stenosis is detected, but experts' opinions are different and varied. Some authors are questioning if carotid endarterectomy (CEA) is an effective strategy for stroke prevention in ACS, supporting best medical treatment (BMT) as therapy alone,[2] while others defend the thesis of plaque progression toward symptomatology in a significant percentage of cases notwithstanding contemporary BMT.[3] There are also middle ground positions which advocate more balanced indications stressing that, per 1000 CEAs performed in ACS, only 50 strokes are prevented at 5-years.[4]

The identification of high-risk plaque conditions, which considers the degree of carotid stenosis in addition to the composition of the plaque,[5] could have strong prognostic implications. The concept of plaque vulnerability has evolved over the years, informed by both clinical experience and radiological studies.[6, 7] Irregular, heterogeneous and soft plaques are more frequently correlated with symptoms and, rapid plaque volume progression in severe narrowing.[8]

Computational fluid dynamics (CFD) has been used for the study of carotid blood dynamics to provide indications to guide clinicians.[9-12] To obtain a characterization of blood dynamics and internal structural forces in plaque, several works considered a fluid structure interaction (FSI) approach.[13,14] This described the interaction of blood with the plaque and allowed investigation of different plaque typologies.[15]

The aim of our research was to assess, in ACS patients, the hemodynamic and mechanical behaviors due to different plaque morphologies using FSI analysis empowered by the use of an innovative geometric tool to reconstruct the plaque. [15]

To investigate the plaque behavior, we computed hemodynamic and mechanical quantities related to plaque vulnerability,[16-17] and proposed an innovative indicator based on the plaque energy to stratify the different plaque typologies.

MATERIALS AND METHODS

Selection of patients and imaging reconstruction

Fifteen ACS patients with severe carotid stenosis and candidates for CEA, were selected and submitted to carotid doppler ultrasound (DUS). Preoperative evaluation of the degree of stenosis and plaque typology were performed by a well-trained ultrasonographer (RC). The percentage of stenosis was classified according to the guidelines of the European Society for Vascular Surgery (ESVS).[18]

Lipid plaques (LP), fibrotic plaques (FP) and calcific plaques (CP) have been identified as according to Gray-Weale classification based on plaque echo-lucency.[19]

After DUS, all patients were submitted to computed tomographic angiography (CTA) as a part of the preoperative work-up.

Ethical review board approval and informed consent were obtained from all patients recruited in the study (FLUIDODINAMIC-AUX 34C002_2020).

Geometric reconstruction of lumen, vessel wall and plaque

The surface of the lumen was reconstructed from CTA images with the library VMTK (http://www.vmtk.org/) and then turned into computational fluid meshes. To create the mesh of vessel wall and plaque, we used our previously published geometric tool.[15] We geometrically modeled LP as a plaque of type I, with an external layer composed by a thin fibrous cap with a thickness of about 100 μm;[20] FP was modeled as a plaque of type III, formed only by fibrotic

material,[21] whereas CP as a plaque of type V, with compact and coherent calcifications [22] covered by a thin fibrous cap (Fig. 1).

Fluid-structure interactions analysis

To study the behavior of different plaques, we used a FSI model,[23] where blood was considered as a Newtonian, homogeneous, and incompressible fluid,[24] whereas healthy vessel and plaque components as a linear elastic material. A flow waveform with an average flow rate of 248.5 mL/min, taken from the literature,[25] was assigned at the inlet of the carotid. At each of the outlets, a three element windkessel model [26] was considered to simulate the distal vasculature, calibrated as proposed in Groen et al.,[27] to obtain suitable flow divisions for different degrees of stenosis (Table 1).

For the structure problem, we imposed null displacements at the inlet and outlet rings, whereas on the external surface, we applied a set of elastic springs to mimic the surrounding tissue.[28] FSI simulations were performed with the Finite Elements library LifeV (https://bitbucket.org/lifev-dev/lifev-release/wiki/Home).[15] The time step was $1 \cdot 10^{-3}$s, the Young modulus E was 300 KPa for the healthy vessel,[28] 30 KPa for the lipidic core,[29] 300 KPa for the fibrous cap,[29] and 30 MPa for the calcifications.[30]

Quantities of interest

To describe the role of hemodynamics in determining the vulnerability conditions of the plaque, some specific quantities were computed.

Wall Shear Stresses (WSS) represents the magnitude of blood tangential forces on the endothelium, causing a stress within the plaque. High values of WSS could induce plaque rupture.[31] WSS_{syst} is the systolic maximum-in-space WSS.

Displacements (D) of the plaques which provide information about the plaque stability since high displacements are recognized to be a source of instabilities.[32] D_{syst} is the systolic maximum-in-space value of D;

von Mises Stresses (VMS), i.e. structural internal stresses. Areas of the fibrous cap with high values of VMS were correlated with a larger rupture risk.[33] VMS_{syst} is the systolic maximum-in-space VMS;

Absorbed Elastic Energy (AEE) is the mechanical potential energy, per unit of volume, stored in the plaque during elastic deformation. The systolic maximum-in-space AEE is

$$AEE_{syst} = \frac{\left(VM_{syst}\right)^2}{2 \cdot E} \ [J/m^3].$$

RESULTS

A total of 15 carotids were selected from patients submitted to CEA for >70% ACS. Three typologies of plaque (LP, FP and CP) were analyzed (Table 1), see Fig. 2 for the vessel and plaque computational meshes.

We start analyzing the WSS magnitude at the systolic peak (Fig. 3), which resulted significantly high in CP. Accordingly, in FP we found intermediate WSS values, whereas in LP the lowest ones. We computed also the spatial distribution of the displacement magnitude within the plaque (Fig. 4). The highest values were observed for LP group, while the lowest ones for CP. We observed that within the LP group, the maximum values were localized mainly in the inner region of the fibrous cap, at the shoulder of the stenosis, whereas for FP and CP a homogeneous distribution of the displacements around the plaque was observed, with an absence of hotspots.

We then analyzed the spatial distribution of VMS at the systolic peak (Fig. 5). In the LP group the areas with higher VMS were located in the inner region of the fibrous cap, whereas in FP and CP lower values without any concentration of peak stresses were found.

To better quantify the different mechanical behaviors of plaques subjected to blood forces, we reported the distribution of the 100 highest systolic values of WSS, D and VMS clustered in different intervals (Fig. 6). These results confirmed the lowest WSS values for LP and lowest VMS and D values for CP, together with intermediate values for FP for all the quantities.

Considerable attention was paid to determine the spatial distribution of the elastic energy stored by the plaque (Fig. 7). We observed that, in correspondence with the region of the fibrous cap in contact with blood, LP was able to store elevated values of energy. Moreover, the lipidic core absorbed more energy with respect to the calcifications, due to its compliant nature. Table 2 summarizes the values of WSS_{syst}, D_{syst}, VMS_{syst} and AEE_{syst} together with the average values for each type of plaque.

Regarding WSS_{syst}, the average values for LP were 33% and 157% lower than the corresponding values for FP and CP, respectively. An inverse correlation was found for the mechanical quantities: the average value of D_{syst} for LP was 250% and 480% greater than for FP and CP, respectively, whereas VMS_{syst} was 150% and 400% greater, respectively.

Lastly, we determined the average values of AEE_{syst} stored by the plaques. We noticed that the fibrous cap of LP absorbed more (470% to 2240%) energy than FP and CP, respectively, while the lipidic core featured very large values, in average greater by several tens of thousands than in the case of calcifications.

DISCUSSION

Engineering studies of carotid bifurcation have been recognized as valuable methods for studying the development of atherosclerosis,[26] surgical techniques,[12] and restenosis development.[34] To further

improve carotid risk stratification, FSI analyses were used to investigate inter-individual variations in blood dynamics and wall mechanics of carotids. Vulnerable sites included all locations where cycling stress and deformation of the plaque can cause focused tissue damage over an area with an underlying lipid core. Gao et al. investigated the impact of fibrous cap thickness and lipid core volume on VMS.[29] Tao et al. analyzed VMS, pressure and flow velocity values at the sites of maximum carotid stenosis and found that maximum VMS was significantly higher in the vulnerable plaque cohort than in stable plaques.[35]

It is also debated whether calcifications act as stabilizers or as exacerbating factors of focal mechanical stress. Li et al., observed that maximum VMS increased by almost 50% when calcium deposits were located in the fibrous cap.[36] Wong et al., observed that calcifications structurally stabilize the plaque.[37] Mahmoud et al., observed that changes of calcification distribution and size modified stress localization.[38]

Our study confirmed that FSI analysis is a suitable method to analyze the hemodynamic and structural behaviors of carotid plaques. We have compared different plaque typologies by investigating hemodynamic and structural quantities. We proposed a new way to identify the plaque and differentiate its components utilizing imaging data that are commonly acquired for diagnostic purposes in clinical practice. A particular attention was paid to the analysis of structural quantities, such as D, VMS, and AEE, which was proposed here for the first time to be a potential indicator to highlight the behavior of different plaque typologies subjected to blood flow.

Our study revealed that LP manifests the highest values of D, VMS and AEE within the plaque. Accordingly, the stenotic lumen highly deformed, leading to WSS values significantly lower than the other plaques. On the contrary, CP showed the lowest VMS and D, making this type of plaque similar to a rigid wall and the most stable. FP presented an intermediate behavior with displacements lower than those in LP but higher than CP ones.

Our computational results highlighted also a positive correlation between the plaque Young's modulus E and blood forces. Indeed, large values of E lead to small lumen expansion and therefore,

according to Bernoulli's principle, to higher values of WSS, which provoked internal forces within the plaque that could increase its vulnerability. However, looking at Figs. 5 and 6 and Table 2, VMS was highest in LP, where WSS had the lowest values. By observing Fig. 7, we can see that the lipidic core, deformed by the action of blood flow, stored more elastic energy with respect to calcifications, due to its increased compliance (low Young's modulus). This amount of deformation energy is then transmitted to the fibrous cap, leading to a localized increase of mechanical stresses, [39] especially in the area between the lumen and the lipidic core. This mechanism can explain why LP featured the highest values of VMS. On the contrary, the calcification was able to transmit only a small quantity of deformation energy to the covering fibrous cap, due to its stiff nature (high Young's modulus), thus resulting in lower values for internal forces.[40] Our analysis showed that FP stored more energy than CP but less than LP, leading to intermediate values of VMS. The fibrous tissue provides more structural integrity to the plaque, compared to the lipidic core.[41]

In summary, these results suggested that different plaque components could act like a spring. Under the action of the blood, they store different amounts of potential mechanical energy, inversely proportional to their elastic modulus, transferring it to the fibrous cap. This amount of deformation is absorbed by the fibrous cap and causes different distribution of internal forces and thus different vulnerability properties. In particular, the lipidic core exerts a key role in making the thin fibrous cap more vulnerable to rupture, leading to the highest values of VMS. Regarding CP, the presence of calcium deposits stabilized the structure by lowering D, AEE, and the internal forces, making the whole plaque less vulnerable.

For all these reasons, our proposal to use the AEE proved to be promising to differentiate the mechanical outcomes of the different plaque typologies in view of assessing their vulnerability.

From a clinical point of view, carotid vulnerability is a multifactorial process that involves, among other factors, the hemodynamics.[42] Indeed, rupture takes place preferentially where the mechanical stress exceeds the ultimate strength of the cap material. In this regard, carotid plaques more prone to be symptomatic usually have lipidic core and thinner fibrous cap.[43]

The management of 60-99% ACS remains a debated matter. The degree of stenosis is the main criterion used to indicate intervention but remains unclear which patients will really benefit from intervention. Kamtchum-Tatuene et al., in a recent meta-analysis on ACS patients, identified that the so defined “high-risk plaque” represented up to 26.5% of cases with an overall incidence of cerebrovascular events higher than currently accepted estimates.[44]

Nicolaides et al., first proposed combining clinical findings with ultrasonographic features in an effort to identify the carotid vulnerable plaques.[45] Naylor et al. tried to determine from the Asymptomatic Carotid Atherosclerosis Study (ACAS) and Asymptomatic Carotid Surgery Trial 1 (ACST-1) predictive algorithms and imaging parameters able to detect the true ACS at risk.[46]

ESVS Clinical guidelines highlighted that the presence of a large juxta-luminal black area on computerized plaque analysis, plaque echo-lucency, or imaging of intra-plaque hemorrhage on MRI, might be useful for the selection of the most proper candidates for CEA.[18]

Our findings led us to some considerations regarding ACS management. Are all the 60-99% ACS harmless? Or should we consider all lipid plaques potentially vulnerable and worthy of preventive surgical treatment? What should be the correct timing for surgery, considering plaque characteristic?

Although some “old” controversies remain in defining the role of surgery in ACS, any effort to better clarify this issue could help determine how to make this important decision.

Limitations

A limitation of this study is related to the absence of any biological evaluation of factors involved in the mechanism of plaque growth and rupture and to the absence of histological or imaging-based analysis of the components of the carotid plaque. However, the aim of the work was precisely to develop a method to be used in absence of such information.

Finally, FSI modeling was performed on plaques considered completely homogenous. The analysis of non-homogeneous carotid plaques will be the object of future work which will analyze how these conditions could impact their properties and vulnerabilities.

CONCLUSIONS

Advances in the comprehension of carotid plaque behavior can develop new methods of assessment for stroke risk prediction based more on the individual setting. FSI studies have denoted that LP experienced huge differences in structural and hemodynamic stresses when compared to FP and CP. Even if the absolute magnitude of these values remains small, however, this stress repeated millions of times could exacerbate the insurgence of plaque disruption and cerebrovascular events. Further prospective studies are needed to validate and quantify these findings, to better stratify plaque vulnerability and to provide robust results useful to identify ACS in more vulnerable subgroups which consequently could benefit from preventive revascularization.

FUNDING

This project has received funding from Istituto Auxologico Italiano: Grant agreement No. 20 07 21 04, FLUIDODINAMIC-AUX.

Acknowledgments

Authors would like to thank Mr. Edward Kiegle for his revision of English grammar and syntax.

REFERENCES

1. Petty G, Brown RD Jr, Whisnant JP, Sicks JD, O'Fallon WM, Wiebers DO. Ischemic stroke subtypes: a population-based study of incidence and risk factors. Stroke. 1999;30:2513–6.

2. Abbott A. Medical (nonsurgical) intervention alone is now best for prevention of stroke associated with asymptomatic severe carotid stenosis: results of a systemic review and analysis. Stroke 2009;40:573-83.

3. Klarin D, Cambria RP, Ergul EA, Silverman SB, Patel VI, LaMuraglia GM, et al. Risk factor profile and anatomic features of previously asymptomatic patients presenting with carotid-related stroke. J Vasc Surg 2018;68:1390-7.

4. Naylor AR. Why is the management of asymptomatic carotid disease so controversial? Surgeon 2015;13:34-43.

5. Paraskevas KI, Cambria RP. Best medical treatment for patients with carotid stenosis: evidence-based medicine or wishful thinking? Angiology. 2018;69:97-9.

6. Freilinger TM, Schindler A, Schmidt C, Grimm J, Clemens C, Schwartz F et al. Prevalence of nonstenosing, complicated atherosclerotic plaques in cryptogenic stroke. JACC Cardiovasc Imaging 2012;5:397–405

7. Seeger JM, Klingman N. The relationship between carotid plaque composition and neurologic symptoms. J Surg Res. 1987;43:78–85.

8. Zhao XQ, Hatsukami TS. Risk factors for development of carotid plaque components. JACC Cardiovasc Imaging. 2018;11:193–5.

9. Milner JS, Moore JA, Rutt BK, Steinman DA. Hemodynamics of human carotid artery bifurcations: Computational studies with models reconstructed from magnetic resonance imaging of normal subjects. J Vasc Surg 1998;28:143-56.

10. Kamenskiy AV, Pipinos II, MacTaggart JN, Kazmi SA, Dzenis YA. Comparative analysis of the biaxial mechanical behavior of carotid wall tissue and biological and synthetic materials used for carotid patch angioplasty. J Biomech Eng 2011;133:111008.

11. Domanin M, Buora A, Scardulla F, Guerciotti B, Forzenigo L, Biondetti P et al. Computational fluid-dynamic analysis after carotid endarterectomy: patch graft versus direct suture closure. Ann Vasc Surg.

2017;44:325-35.

12. Domanin M, Bissacco D, Le Van D, Vergara C. Computational fluid dynamic comparison between patch-based and primary closure techniques after carotid endarterectomy. J Vasc Surg. 2018;67:887–97.

13. Tang D, Yang C, Zheng J, Woodard PK, Saffitz JE, Sicard GA, Pilgram TK, Yuan C. Quantifying effects of plaque structure and material properties on stress distributions in human atherosclerotic plaques using 3D FSI models. J. Biomech. Eng. 2005;127:1185–94.

14. Yang C, Canton G, Yuan C, Ferguson M, Hatsukami TS, Tang D. Advanced human carotid plaque progression correlates positively with flow shear stress: an in vivo MRI multi-patient 3D FSI study. J. Biomech. 2010;43: 2530–8.

15. Bennati L, Vergara C, Domanin M, Malloggi C, Bissacco D, Trimarchi S et al. A computational fluid structure interaction study for carotids with different atherosclerotic plaques. J Biomech Eng. 2021 (in press).

16. Naim C, Douziech M, Therasse E, Robillard P, Giroux MF, Arsenault F et al. Vulnerable atherosclerotic carotid plaque evaluation by ultrasound, computed tomography angiography, and magnetic resonance imaging: an overview. Can Assoc Radiol J. 2014;65:275-86.

17. Li ZY, Howarth SP, Tang T, Graves MJ, U-King-Im J, Trivedi RA et al. Structural analysis and magnetic resonance imaging predict plaque vulnerability: a study comparing symptomatic and asymptomatic individuals. J Vasc Surg. 2007;45:768-75.

18. Naylor AR, Ricco JB, de Borst GJ, Debus S, de Haro J, Halliday A, et al. Editor’s choice - management of atherosclerotic carotid and vertebral artery disease: 2017 clinical practice guidelines of the European Society for Vascular Surgery (ESVS). Eur J Vasc Endovasc Surg 2018;55:3e81.

19. Gray-Weale AC, Graham JC, Burnett JR, Bryne K, Lusby RJ. Carotid artery atheroma: comparison of preoperative B-mode ultrasound appearance with carotid endarterectomy specimen pathology. J Cardiovasc Surg. 1988;2:676–81.

20. Li Z-Y, Howarth SP, Tang T, Gillard JH. How critical is fibrous cap thickness to carotid plaque stability? Stroke. 2006;37:1195–9.

21. Thrysøe SA, Oikawa M, Yuan C, Eldrup N, Klaerke A, Paaske WP et al. Longitudinal distribution of mechanical stresses in carotid plaques of symptomatic patients. Stroke. 2010;41:1041-3.

22. Friedrich GJ, Moes NY, Muhlberger VA, Gabl C, Mikuz G, Hausmann D et al. Detection of intralesional calcium by intracoronary ultrasound depends on the histologic pattern. Am Heart Journ. 1994;128:435–41.

23. Quarteroni A, Manzoni A, Vergara C. The cardiovascular system: Mathematical modelling, numerical algorithms and clinical applications. Acta Numerica. 2017;26:365–590.

24. Perktold K, Resch M. Numerical flow studies in human carotid artery bifurcations: basic discussion of the geometric factor in atherogenesis. Biomed Eng. 1990;12:111-23.

25. Guerciotti B, Vergara C, Azzimonti L, Forzenigo L, Biondetti P, Domanin M. Computational study of the fluid-dynamics in carotids before and after endarterectomy. J Biomech. 2016;49:26-38.

26. Quarteroni A, Veneziani A, Vergara C. Geometric multiscale modeling of the cardiovascular system, between theory and practice. Comput. Methods Appl. Mech. Engrg. 2016;302:193–252.

27. Groen HC, Simons L, Van Den Bouwhuijsen QJ, Bosboom EM, Gijsen FJ, van der Giessen AG et al. MRI-based quantification of outflow boundary conditions for computational fluid dynamics of stenosed human carotid arteries. J Biomech. 2010;43:2332-8.

28. Pozzi S, Domanin M, Forzenigo L, Votta E, Zunino E, Redaelli A et al. A surrogate model for plaque modeling in carotids based on Robin conditions calibrated by cine MRI data. Int J Numer Method Biomed Eng. 2021 Feb 14:e3447.

29. Gao H, Long Q. Effects of varied lipid ore volume and fibrous cap thickness on stress distribution in carotid arterial plaques. J Biomech. 2008;41:3053–9.

30. O'Reilly BL, Hynes N, Sultan S, McHugh P.E, McGarry JP. An experimental and computational investigation of the material behaviour of discrete homogenous iliofemoral and carotid atherosclerotic plaque constituents. J Biomech. 2020:106;1–9.

31. Groen H, Gijsen F, Lugt A, Ferguson M, Hatsukami T, van der Steen A et al. Plaque rupture in the carotid artery is localized at the high shear stress region: a case report. Stroke. 2007;38:2379–81.

32. Bang J, Dahl T, Bruinsma A, Kaspersen J, Hernes T, Myhre H. A new method for analysis of motion of carotid plaques from RF ultrasound images. Ultrasound Med Biol 2003;29:967–76.

33. Ohayon J, Finet G, Gharib AM, Herzka DA, Tracqui P. Necrotic core thickness and positive arterial remodeling index: emergent biomechanical factors for evaluating the risk of plaque rupture. Am J Physiol Heart Circ Physiol. 2008; 295:H717–H727.

34. Domanin M, Gallo D, Vergara C, Biondetti P, Forzenigo L, Morbiducci U. Prediction of long-term restenosis risk after surgery in the carotid bifurcation by hemodynamic and geometric analysis. Ann Biomed Eng. 2019;47:1129–40.

35. Tao X, Gao P, Jing L, Lin Y, Sui B. Subject-specific fully-coupled and one-way fluid- structure interaction models for modeling of carotid atherosclerotic plaques in humans. Med Sci Monit. 2015;21:3279–90.

36. Li ZY, Howarth S, Tang T, Graves M, U-King-Im J, Gillard JH. Does calcium deposition play a role in the stability of atheroma? Location may be the key. Cerebrovasc. 2007;24:452-9.

37. Wong KK, Thavornpattanapong P, Cheung SC, Sun Z, Tu J. Effect of calcification on the mechanical stability of plaque based on a three-dimensional carotid bifurcation model. BMC Cardiovasc Disord. 2012;7.

38. Mahmoud AH, Hassan N, Mahmoud AM. Three-dimensional fluid structure interaction analysis of carotid artery models with different calcification patterns. 41st Annual International Conference of the IEEE Engineering in Medicine and Biology Society, Berlin, Germany, 2019, 7019-22. doi: 10.1109/EMBC.2019.8856813.

39. Pedrigi RM, de Silva R, Bovens SM, Mehta VV, Petretto E, Krams R. Thin-cap fibroatheroma rupture is associated with a fine interplay of shear and wall stress. Arterioscler Thromb Vasc Biol. 2014;34:2224-31.

40. Richardson PD. Biomechanics of plaque rupture: progress, problems, and new frontiers. Ann Biomed Eng. 2002;30:524-36.

41. van der Wal AC, Becker AE. Atherosclerotic plaque rupture--pathologic basis of plaque stability and instability. Cardiovasc Res. 1999;41:334-44.

42. Casscells W, Naghavi M, Willerson JT. Vulnerable atherosclerotic plaque: a multifocal disease. Circulation. 2003;107:2072–5.

43. Redgrave JN, Lovett JK, Rothwell PM. Histological features of symptomatic carotid plaques in relation to age and smoking: the Oxford plaque study. Stroke. 2010;41:2288–94.

44. Kamtchum-Tatuene J, Noubiap JJ, Wilman AH, Saqqur M, Shuaib A, Jickling GC. Prevalence of high-risk plaques and risk of stroke in patients with asymptomatic carotid stenosis: A Meta-analysis. JAMA Neurol. 2020 Aug 3:e202658.

45. Nicolaides AN, Kakkos SK, Kyriacou E, Griffin M, Sabetai M, Thomas DJ, et al. Asymptomatic internal carotid artery stenosis and cerebrovascular risk stratification. J Vasc Surg 2010;52:1486-96.
46. Naylor AR, Schroeder TV, Sillesen H. Clinical and imaging features associated with an increased risk of late stroke in patients with asymptomatic carotid disease. Eur J Vasc Endovasc Surg. 2014;48:633-40.

Table 1. Dataset of the population under investigation. Q_{ICA}= Flux of Internal Carotid Artery; Q_{CCA}= Flux of the Common Carotid Artery.

Patient	Age	Sex	% of stenosis	Type of plaque	Q_{ICA}/Q_{CCA}
LP1	62	M	75	Lipidic	0.7
LP2	71	M	75	Lipidic	0.7
LP3	81	M	80	Lipidic	0.625
LP4	84	M	85	Lipidic	0.55
LP5	82	M	90	Lipidic	0.475
FP1	74	M	75	Fibrous	0.7
FP2	84	M	85	Fibrous	0.55
FP3	66	M	90	Fibrous	0.475
FP4	84	M	90	Fibrous	0.475
FP5	83	M	90	Fibrous	0.475
CP1	84	M	80	Calcific	0.625
CP2	61	F	80	Calcific	0.625
CP3	61	F	85	Calcific	0.55
CP4	68	F	90	Calcific	0.475
CP5	74	F	90	Calcific	0.475

Table 2. Values of WSS_{syst} at the stenosis, D_{syst}, VMS_{syst} and AEE_{syst} within the fibrous cap and within the plaque component. Average values of all the quantities for each type of plaque are also presented.

Patient	WSS_{syst} [Pa]	Average [Pa]	D_{syst} [mm]	Average [mm]	VMS_{syst} [KPa]	Average [KPa]	AEE_{syst} fibrous cap [J/m^3]	Average [J/m^3]
LP1	63		0.22		41		2800	
LP2	55	79	0.21	0.21	40	37	2666	2320
LP3	76		0.23		36		2160	
LP4	62		0.16		36		2160	
LP5	140		0.22		33		1815	
FP1	66		0.05		13		282	
FP2	118	105	0.08	0.06	18	15 (-150%)	540	408 (-470%)
FP3	116		0.09		14		330	
FP4	117	(+33%)	0.07	(-250%)	14		336	
FP5	110		0.01		18		555	
CP1	98		0.030		6		60	
CP2	120	203	0.032	0.036	5	7.4 (-400%)	42	99 (-2240%)
CP3	140		0.034		8		110	
CP4	282	(+157%)	0.045	(-480%)	9		140	
CP5	377		0.040		9		140	

FIGURES CAPTIONS

Figure 1. Geometric reconstruction of the vessel lumen and of the three types of carotid plaques. Red: healthy vessel; Light blue: fibrous cup; Yellow: lipidic core; Grey: calcifications; Orange: lumen.

Figure 2. Structure meshes were generated by means of our geometric tool [23]. Red: healthy vessel; Light blue: fibrous cup; Yellow: lipidic core; Grey: calcifications; Orange: lumen.

Figure 3. Spatial distribution of wall shear stress (WSS) magnitude at the systolic peak. Top: Lipidic plaques (LP); Middle: Fibrotic plaques (FP); Bottom: Calcific plaques (CP).

Figure 4. Spatial distribution of the magnitude of the plaque structure displacements (D) at systolic peak within the plaque. Top: Lipidic plaques (LP); Middle: Fibrotic plaques (FP); Bottom: Calcific plaques (CP).

Figure 5. Spatial distribution of Von Mises stresses (VMS) at systolic peak within the plaque. Top: Lipidic plaque (LP); Middle: Fibrotic plaques (FP); Bottom: Calcific plaques (CP).

Figure 6. Distribution of the 100 highest values for WSS (a), D (b) and plaque VMS (c) for all the different plaques at the systolic peak. Values are intended as magnitudes of the corresponding field.

Figure 7. Spatial distribution of the Absorbed Elastic Energy (AEE) at the systolic peak, during the deformation of the fibrous cap and of the lipidic core and calcifications. Top: Lipidic plaques; Middle: Fibrous plaques; Down: Calcific plaques. Legend on the left refers to the distribution in the fibrous part reported over sections around the stenotic lumen; legend on the right refers to the lipidic and calcified parts reported over the internal plaque surface.

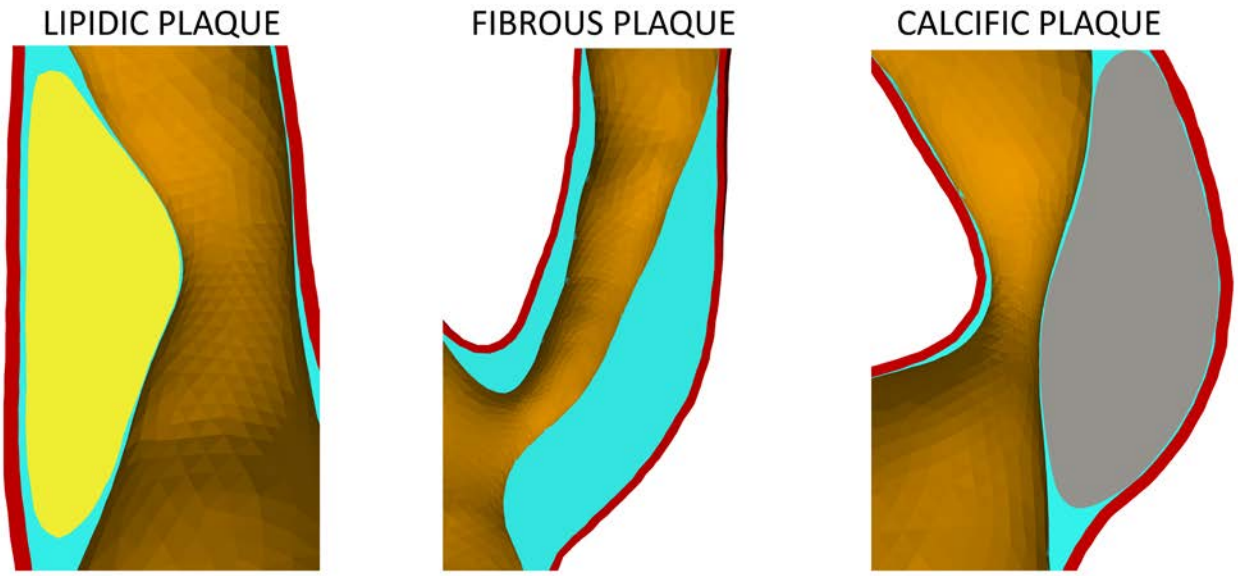

Fig. 1

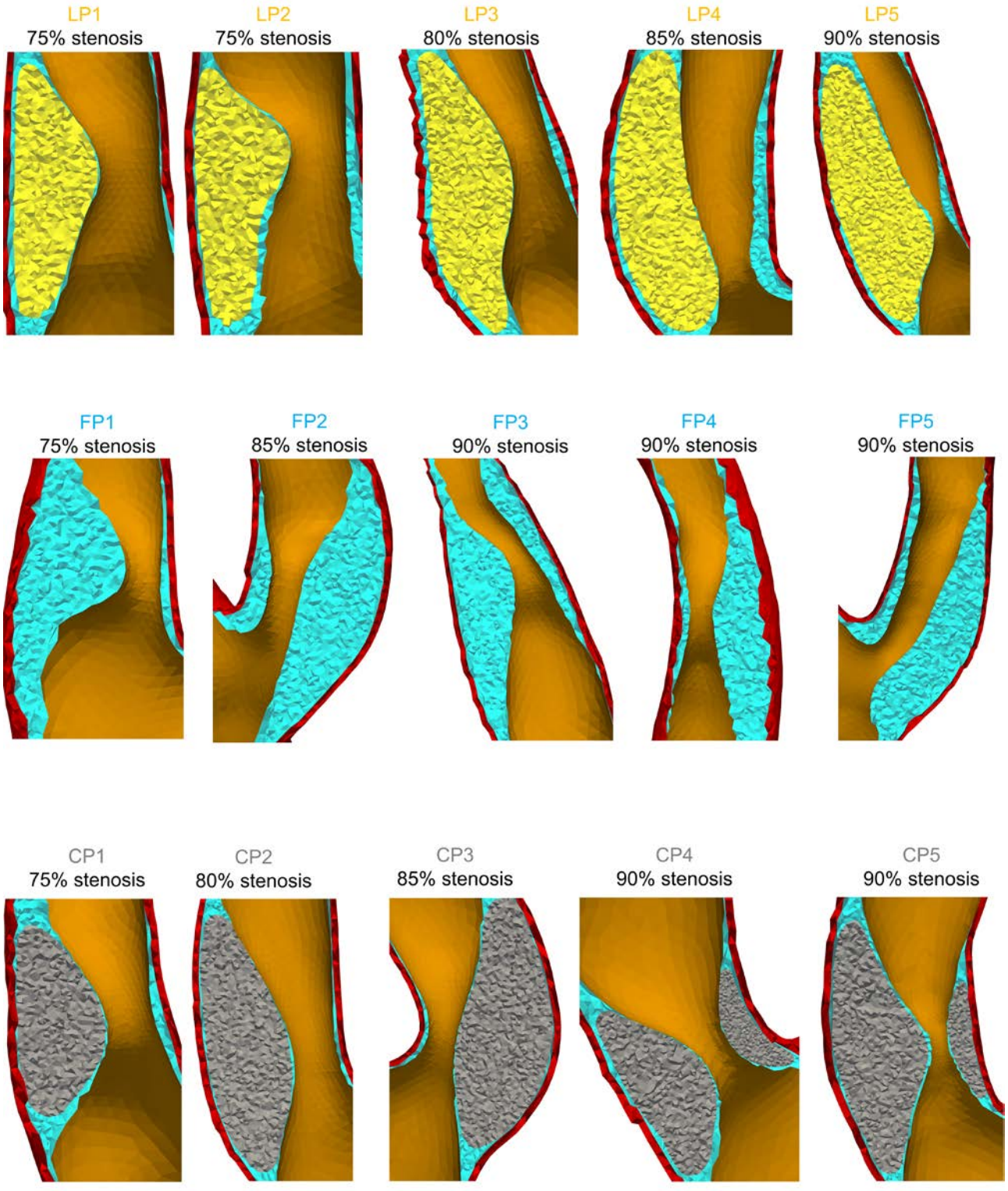
LP1
75% stenosis
LP2
75% stenosis
LP3
80% stenosis
LP4
85% stenosis
LP5
90% stenosis
FP1
75% stenosis
FP2
85% stenosis
FP3
90% stenosis
FP4
90% stenosis
FP5
90% stenosis
CP1
75% stenosis
CP2
80% stenosis
CP3
85% stenosis
CP4
90% stenosis
CP5
90% stenosis

Fig. 2

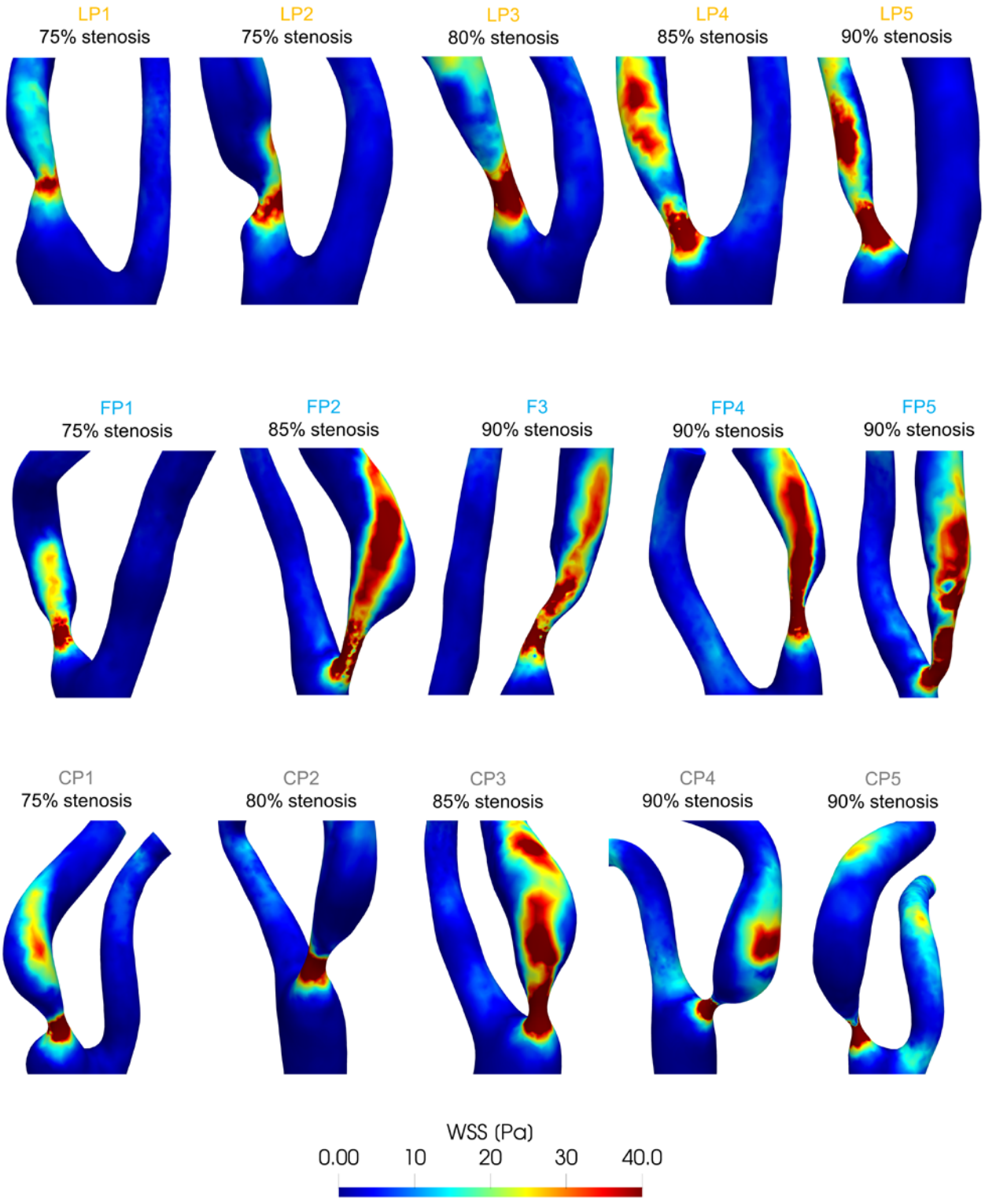
LP1
75% stenosis
LP2
75% stenosis
LP3
80% stenosis
LP4
85% stenosis
LP5
90% stenosis
FP1
75% stenosis
FP2
85% stenosis
F3
90% stenosis
FP4
90% stenosis
FP5
90% stenosis
CP1
75% stenosis
CP2
80% stenosis
CP3
85% stenosis
CP4
90% stenosis
CP5
90% stenosis
WSS (Pa)
0.00
10
20
30
40.0

Fig. 3

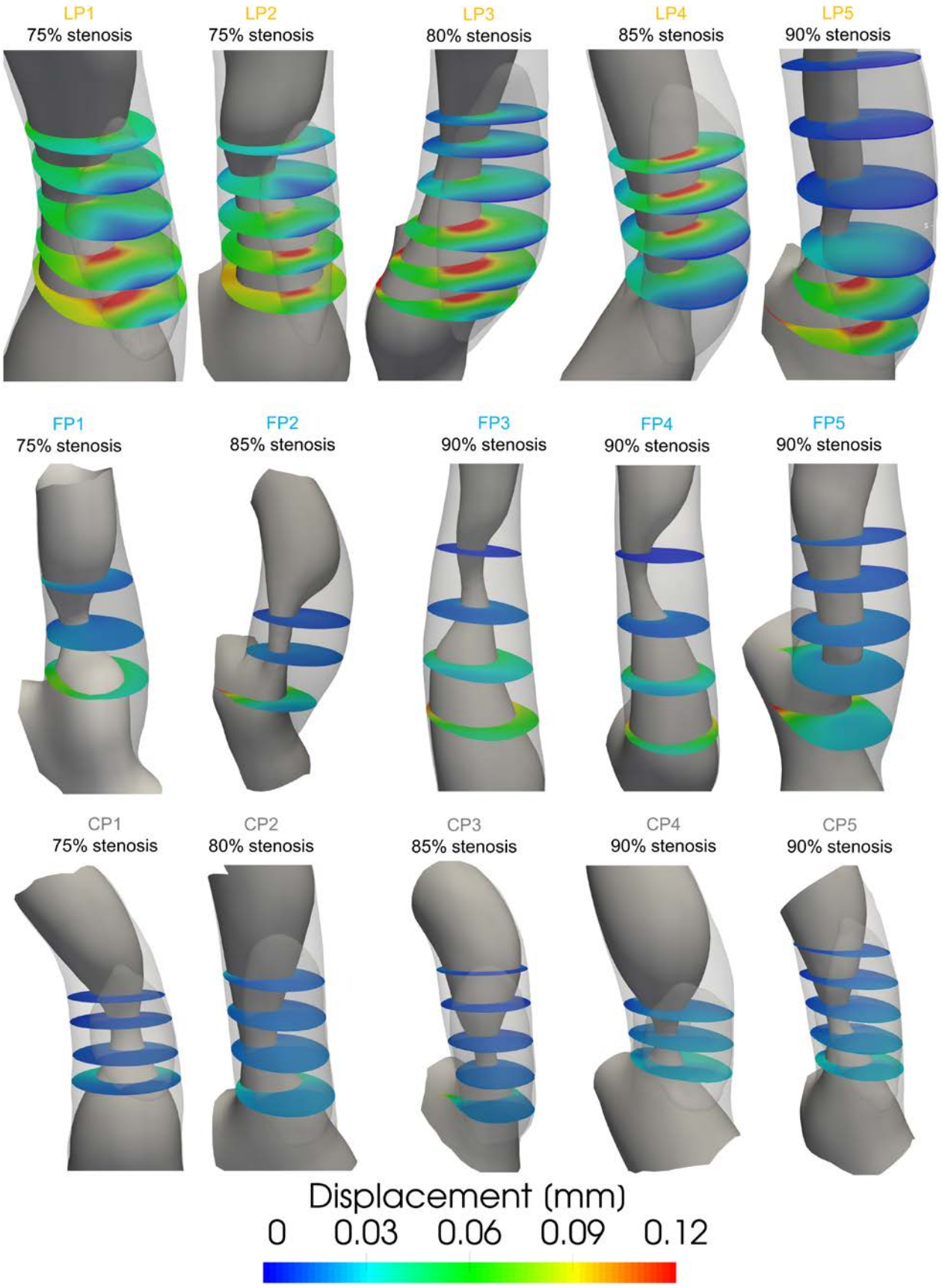
LP1
75% stenosis
LP2
75% stenosis
LP3
80% stenosis
LP4
85% stenosis
LP5
90% stenosis
FP1
75% stenosis
FP2
85% stenosis
FP3
90% stenosis
FP4
90% stenosis
FP5
90% stenosis
CP1
75% stenosis
CP2
80% stenosis
CP3
85% stenosis
CP4
90% stenosis
CP5
90% stenosis
Displacement (mm)
0 0.03 0.06 0.09 0.12

Fig. 4

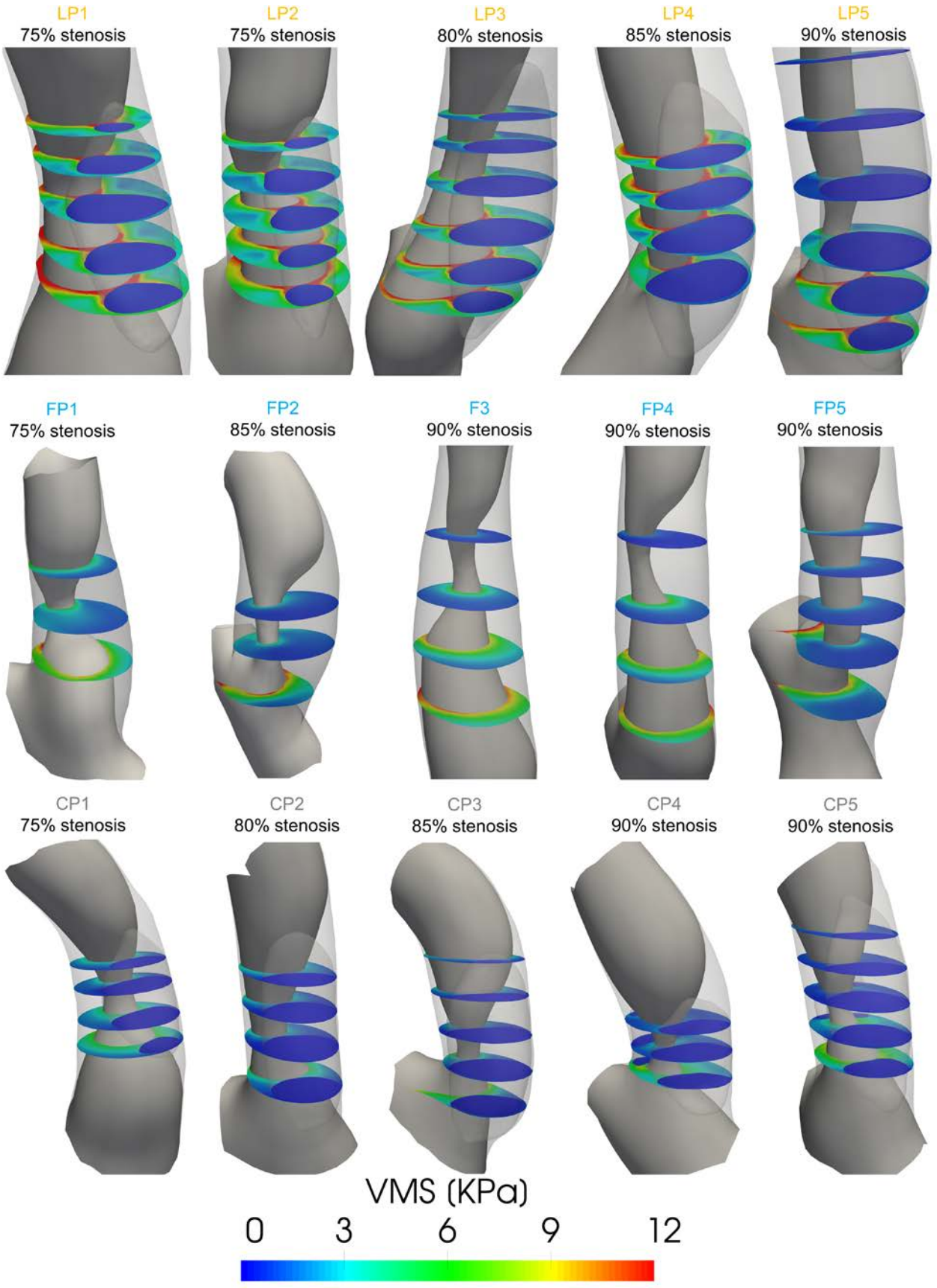
LP1
75% stenosis
LP2
75% stenosis
LP3
80% stenosis
LP4
85% stenosis
LP5
90% stenosis
FP1
75% stenosis
FP2
85% stenosis
F3
90% stenosis
FP4
90% stenosis
FP5
90% stenosis
CP1
75% stenosis
CP2
80% stenosis
CP3
85% stenosis
CP4
90% stenosis
CP5
90% stenosis
VMS (KPa)
0
3
6
9
12

Fig. 5

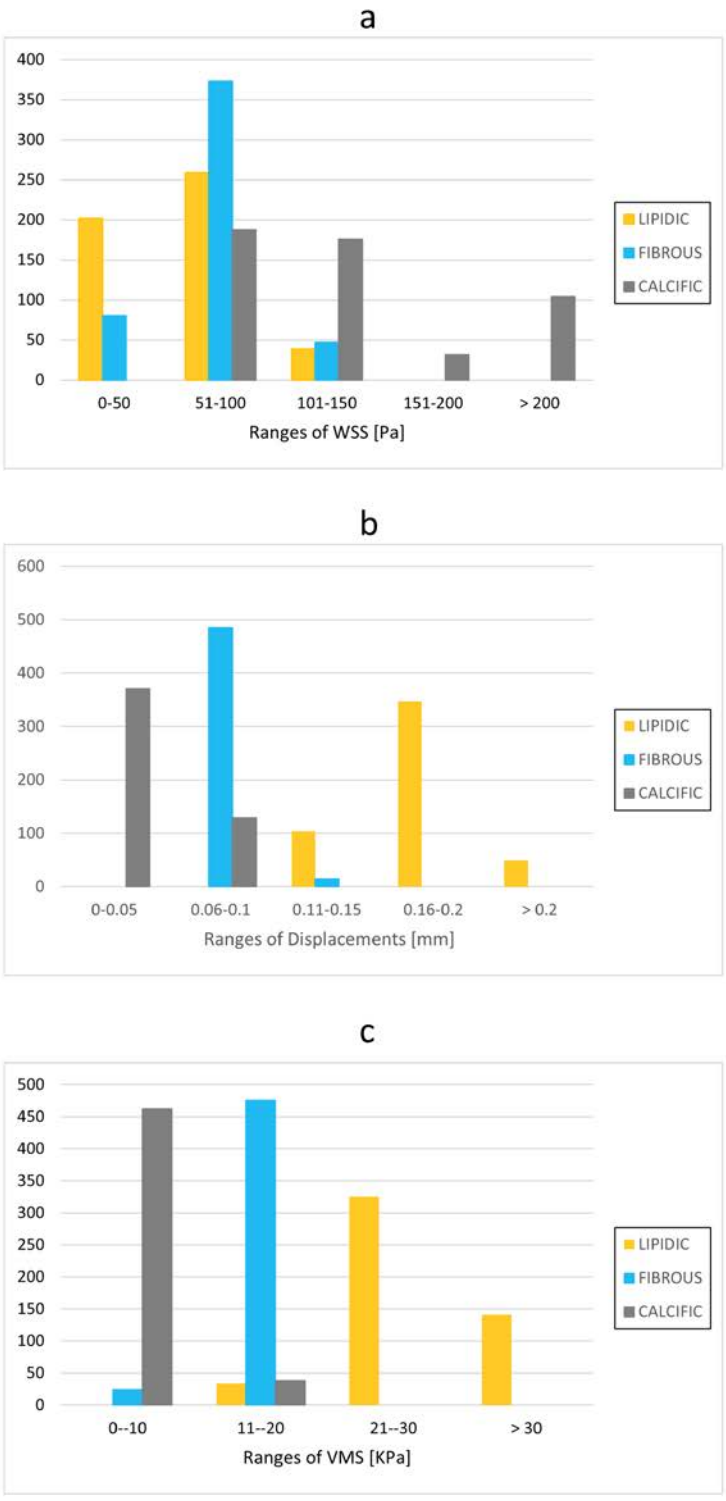
a
400
350
300
250
200
150
100
50
0
0-50
51-100
101-150
151-200
> 200
Ranges of WSS [Pa]
LIPIDIC
FIBROUS
CALCIFIC
b
600
500
400
300
200
100
0
0-0.05
0.06-0.1
0.11-0.15
0.16-0.2
> 0.2
Ranges of Displacements [mm]
LIPIDIC
FIBROUS
CALCIFIC
c
500
450
400
350
300
250
200
150
100
50
0
0--10
11--20
21--30
> 30
Ranges of VMS [KPa]
LIPIDIC
FIBROUS
CALCIFIC

Fig. 6

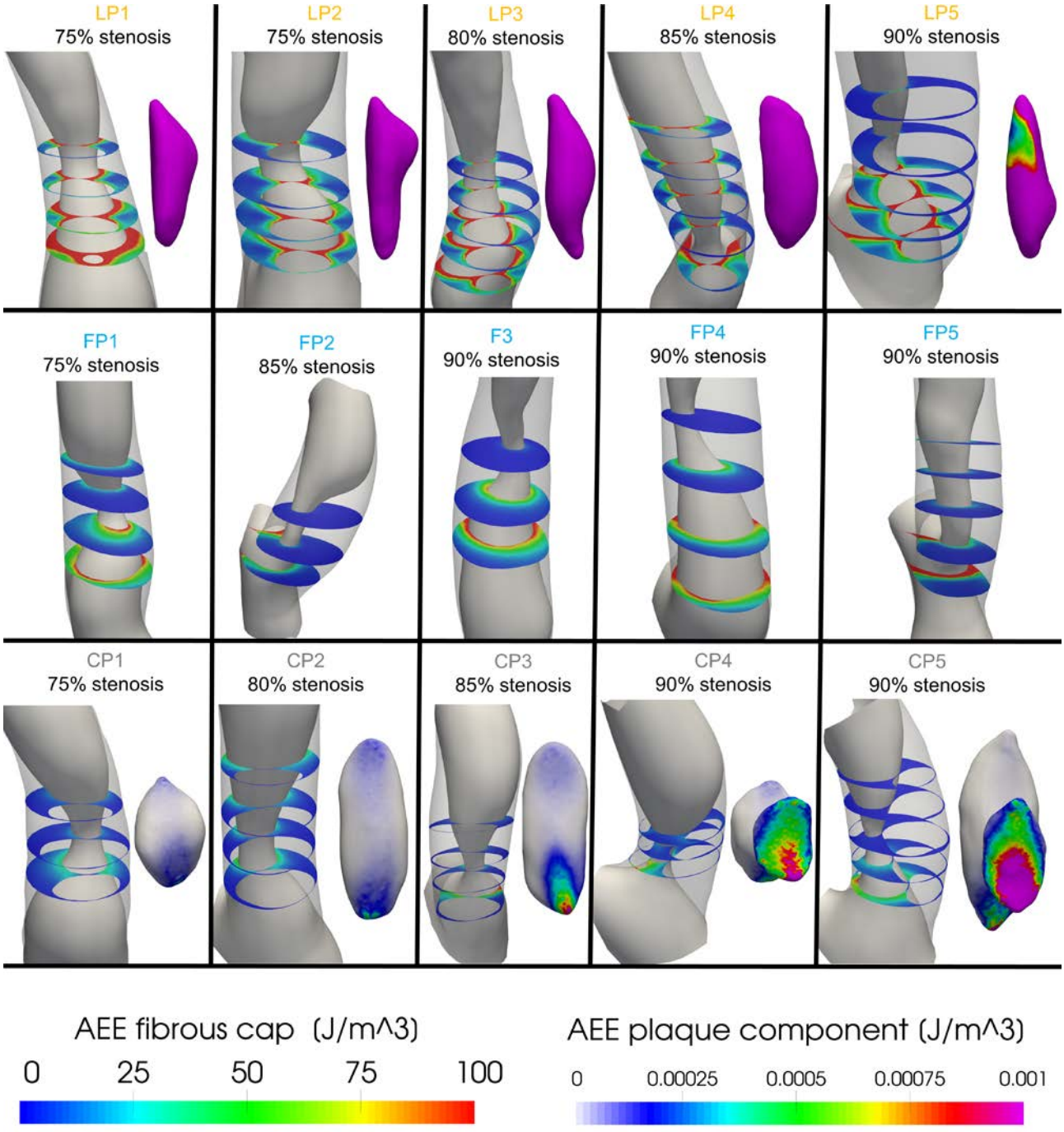
LP1
75% stenosis
LP2
75% stenosis
LP3
80% stenosis
LP4
85% stenosis
LP5
90% stenosis
FP1
75% stenosis
FP2
85% stenosis
F3
90% stenosis
FP4
90% stenosis
FP5
90% stenosis
CP1
75% stenosis
CP2
80% stenosis
CP3
85% stenosis
CP4
90% stenosis
CP5
90% stenosis
AEE fibrous cap (J/m^3)
0
25
50
75
100
AEE plaque component (J/m^3)
0
0.00025
0.0005
0.00075
0.001

Fig. 7

SUPPLEMENTARY MATERIAL

Computational fluid meshes was composed of about 220k tetrahedra with 3 boundary layers. This corresponds to a representative value of the space discretization of about 0.05 cm far from the stenosis and about 0.01 cm at the stenosis. These values were based on a mesh convergence analysis that showed that further mesh refining would have produced a negligible difference in the computed WSS. The structure (healthy vessel and plaque) meshes were composed of about 300k tetrahedra. The value of the space discretization parameters was set to 0.1 cm for all structure meshes.

MOX Technical Reports, last issues

Dipartimento di Matematica
Politecnico di Milano, Via Bonardi 9 - 20133 Milano (Italy)

20/2021 Pasquale, A.; Ammar, A.; Falcó, A.; Perotto, S.; Cueto, E.; Duval, J.-L.; Chinesta, F.
A separated representation involving multiple time scales within the Proper Generalized Decomposition framework

21/2021 Torti, A.; Galvani, M.; Menafoglio, A.; Secchi, P.; Vantini S.
A General Bi-clustering Algorithm for Hilbert Data: Analysis of the Lombardy Railway Service

19/2021 Gillard, M.; Benacchio, T.
FT-GCR: a fault-tolerant generalized conjugate residual elliptic solver

18/2021 Gigante, G.; Vergara, C.
On the choice of interface parameters in Robin-Robin loosely coupled schemes for fluid-structure interaction

17/2021 Chew, R.; Benacchio, T.; Hastermann, G.; Klein, R.
Balanced data assimilation with a blended numerical model

16/2021 Salvador, M.; Dede', L.; Manzoni, A.
Non intrusive reduced order modeling of parametrized PDEs by kernel POD and neural networks

13/2021 Ferro, N.; Perotto, S.; Cangiani, A.
An anisotropic recovery-based error estimator for adaptive discontinuous Galerkin methods

14/2021 Peli, R.; Menafoglio, A.; Cervino, M.; Dovera, L.; Secchi, P;
Physics-based Residual Kriging for dynamically evolving functional random fields

15/2021 Fumagalli, A.; Patacchini, F.S.
Model adaptation in a discrete fracture network: existence of solutions and numerical strategies

12/2021 di Cristofaro, D.; Galimberti, C.; Bianchi, D.; Ferrante, R.; Ferro, N.; Mannisi, M.; Perotto, S
Adaptive topology optimization for innovative 3D printed metamaterials